Dalton Transactions

ROYAL SOCIETY OF CHEMISTRY

PAPER

View Article Online
View Journal | View Issue

Cite this: *Dalton Trans.*, 2024, **53**, 467

Molar excess of coordinating N-heterocyclic carbene ligands triggers kinetic digestion of gold nanocrystals†

Neda Arabzadeh Nosratabad, ‡[a] Zhicheng Jin,§[a] Hesam Arabzadeh, ¶[a] Banghao Chen,[a] Cheng Huang[b] and Hedi Mattoussi *[a]

Received 12th September 2023,
Accepted 21st November 2023

DOI: 10.1039/d3dt02961a

rsc.li/dalton

There has been much interest in evaluating the strength of the coordination interactions between N-heterocyclic carbene (NHC) molecules and transition metal ions, nanocolloids and surfaces. We implement a top-down core digestion test of Au nanoparticles (AuNPs) triggered by incubation with a large molar excess of poly(ethylene glycol)-appended NHC molecules, where kinetic dislodging of surface atoms and formation of NHC–Au complexes progressively take place. We characterize the structure and chemical nature of the generated PEG-NHC–Au complexes using 1D and 2D ^{1}H–^{13}C NMR spectroscopy, supplemented with matrix assisted laser desorption/ionization mass spectrometry, and transmission electron microscopy. We further apply the same test using thiol-modified molecules and find that though etching can be measured the kinetics are substantially slower. We discuss our findings within the classic digestion of transition metal ores and colloids induced by interactions with sodium cyanide, which provides an insight into the strength of coordination between the strong σ-donating (soft Lewis base) NHC and Au surfaces (having a soft Lewis acid character), as compared to gold-to-gold covalent binding.

Introduction

Since they were first identified by A. J. Arduengo and co-workers,[1,2] N-heterocyclic carbenes (NHCs) have generated tremendous interest in the past three decades as versatile metal coordinating groups, and they have been actively explored in the area of surface science and catalysis.[3–9] The stability of the carbene center, in NHC-containing molecules, is ascribed to a combination of steric and electronic considerations.[10,11] More precisely, stabilization of NHC groups is controlled by the π-donor nitrogen atoms adjacent to the C_2 carbon, which increases electron density and partially saturates the electronic deficiency of the carbene center. Additionally, the *N*-substituents play an important role by sterically hindering dimerization of imidazole rings to the corresponding olefin.[3,12] These factors can impact the catalytic properties of NHC-metal complexes and NHC-stabilized metal nanoparticles and nanoclusters.[13–17]

Due to the inherent electron-donating nature of the group, a typical NHC-containing molecule is considered a soft Lewis base. It thus exhibits strong coordination interactions (*via* soft-to-soft) with transition metal ions and metallic nanocolloids and surfaces, which present a Lewis acid character.[3] As such, NHC-appended molecules have widely been exploited for the surface passivation and stabilization of a variety of colloidal nanomaterials, including those made of Ru, Pd, Ni, Au, and semiconducting cores.[18–31]

Among metallic nanostructures, gold nanocolloids (*e.g.*, gold nanoparticles, AuNPs, and gold nanorods, AuNRs) possess several unique size- and shape-dependent surface plasmon resonance (SPR) properties combined with large surface-to-volume ratios.[32–34] The above features have generated much interest for using Au nanocolloids in an array of applications ranging from energy transfer processes, catalysis to biomedicine.[35–42] The nature and affinity of surface capping ligands play a crucial role in imparting colloidal stability to these materials. They also permit control over the coating uniformity and NP reactivity. Thiol-based ligands have been routinely employed for the stabilization and functionalization of

[a]*Florida State University, Department of Chemistry and Biochemistry, 95 Chieftan Way, Tallahassee, FL 32306, USA. E-mail: mattoussi@chem.fsu.edu*
[b]*Florida State University, Department of Scientific Computing, Tallahassee, FL 32306, USA*

†Electronic supplementary information (ESI) available: Information on materials, instrumentation, ligand synthesis, characterization data, and supplementary figures. See DOI: https://doi.org/10.1039/d3dt02961a

‡Present address: University of Missouri, Department of Chemical and Biomedical Engineering, Columbia, MO 65201, USA
§Present address: Department of NanoEngineering, University of California, San Diego, La Jolla, CA 92093, USA.
¶Present address: University of Missouri, Department of Chemistry, Columbia, MO 65211, USA.

AuNPs, and high packing density of thiol-appended ligands on Au surfaces has been reported.[43] However, the Au–S bond is prone to oxidation under sample exposure to air, which can lead to ligand desorption and negatively affects the stability of thiol-stabilized colloidal dispersions.[44,45] Several studies have proposed that coordination of NHC molecules onto gold NPs and surfaces provides a few key benefits, and experimental data have reported that the Au–$C_{carbene}$ bond energy is stronger than its Au–S counterpart, *i.e.*, ~158 kJ mol^{-1} (for NHC) *vs.* ~126 kJ mol^{-1} (for SH).[3,11,19,46–49] We should note that larger energy values for those bonds have been predicted in the literature based on DFT and other computational studies.[50] This makes NHC-containing molecules promising ligand candidates for the surface stabilization of Au nanostructures. It has been reported that substituting weakly bonded ligands with NHC-based molecules on AuNPs can dislodge some of the surface Au atoms. This triggers atom rearrangement on the NP surfaces.[51] For instance, experimental and theoretical studies investigating the reactivity of AuNPs towards NHC ligands carried out by Richeter and co-workers have demonstrated that reaction of AuNPs with benzimididazol-2 ylidene ligands causes Au surface reconstruction which leads to the formation of well-defined mono- and biscarbene gold(I) complexes.[51,52] Similarly, Chechik and co-workers reported that substituting the native coating of Au or Pd NPs with bis-*tert*-butylimidazol-2-ylidene ligands promoted leaching of NHC–metal complexes from the NP surfaces. They applied ESI-MS spectrometry analysis to confirm the presence of such NHC–metal complexes.[53] Subsequently, Fuchs, Glorius and co-workers reported that samples prepared *via* physical vapor deposition of NHC molecules onto a planar gold substrate (*i.e.*, under ultrahigh vacuum), also produce mobile NHC–Au adatoms.[54]

Here, we implement a simple experiment aimed at testing whether or not the proposed rationale that a good match between the soft Lewis base NHC with the soft Lewis acid character of the AuNP surfaces would yield coordination interactions that are strong enough to equal or surpass the covalent Au-to-Au binding. For this, dispersions of pre-grown hydrophobic AuNPs (10 nm diameter), with a native oleylamine (OLA) coating, have been mixed with monomeric polyethylene glycol (PEG)-appended NHC (NHC-PEG) ligands in large excess, then the mixture is left to incubate for an extended period of time, as schematically represented in Fig. 1A. The UV-vis absorption profiles for several samples with varying ligand molar excess, with respect to the NPs, have been recorded for a total period spanning anywhere from a few hours to several days. We find that using molar excess of NHC-PEG induces a progressive top-down etching (or digestion) of the AuNPs, manifesting in progressive loss of the SPR feature, ultimately leading to the disappearance of the plasmonic signature of the nanocolloids and loss of the characteristic pinkish/red color of the dispersions. Data also show that the kinetics of etching strongly depend on the ligand molar excess used. We combine 1D ^{1}H and ^{13}C, 2D ^{1}H–^{13}C Heteronuclear Multiple Bond Correlation (HMBC) NMR spectroscopy, matrix assisted laser desorption/ionization (MALDI) mass spectrometry, and transmission electron microscopy (TEM) to characterize the products generated under these conditions.

Results and discussion

The rationale used for developing the present experimental design to assess the strength of the coordination interactions between NHC molecules and AuNPs is based on a few key findings. (1) Literature data have shown that even though NHC-modified molecules strongly coordinate (through two-electron σ-donating orbitals) onto metallic surfaces, particularly AuNPs, they are not capable of providing a dense and rigid surface capping layer.[54] (2) We have previously tested the strength of NHC-to-Au colloids by designing a multi-NHC polymer bearing hydrophilic motifs.[29] The polymer, referred to as NHC-PIMA-PEG (Fig. 1C), was prepared by installing several NHC groups and multiple polyethylene glycol (PEG) blocks along a polymer backbone, *via* ring opening reaction between poly (isobutylene maleic anhydride) copolymer (PIMA) and amine-NHC and amine-PEG.[55] We found that ligand exchange of OLA-coated AuNPs with the NHC-polymer, followed by purification of the sample by removing the native ligands and excess free NHC-polymer, yielded homogenous hydrophilic dispersions that exhibit long term colloidal stability under a few biologically relevant conditions for over one year, as reported in ref. 29. We have subsequently tracked those same dispersions after longer storage period. White light images along with UV-vis absorption profiles acquired from those samples after ~4 years show homogeneous dispersions with no change in the SPR features (see Fig. 1B). Furthermore, dynamic light scattering measurements acquired from those samples show one population of intensity *vs.* hydrodynamic size histograms (extracted from the Laplace transform of the scattered laser signals) for all samples. Given the sensitivity of the C_2 carbon to water (a harsh venue for such group), our findings imply that appending multiple NHC groups along the polymer chain produces added stability to the NHC–Au coordination, which drastically reduces the rate of ligand desorption. This in turn limits exposure of intact NHCs to the surrounding water environment and prevents protonation of the C_2, resulting in extended colloidal stability for the AuNP dispersions. (3) The present study draws from the use of sodium cyanide (NaCN) digestion test, applied to hydrophilic dispersions of AuNPs and Au nanorods (AuNRs) under varying conditions, to ascertain the effectiveness of a given surface coating strategy to reduce the cyanide-induced digestion of the nanocolloids. In this case, dissolution of the salt (in water) yields CN^{-} anions that diffuse across the coating to the NP surface where they form cyanide–Au complexes, progressively etching the nanoparticle surfaces and reducing the NP overall dimensions, following a qualitative oxidation chemical reaction of the form:[56–59]

$$4Au(0) + 8NaCN + O_2 + 2H_2O \rightarrow 4Na[Au(CN)_2] + 4NaOH \quad (1a)$$

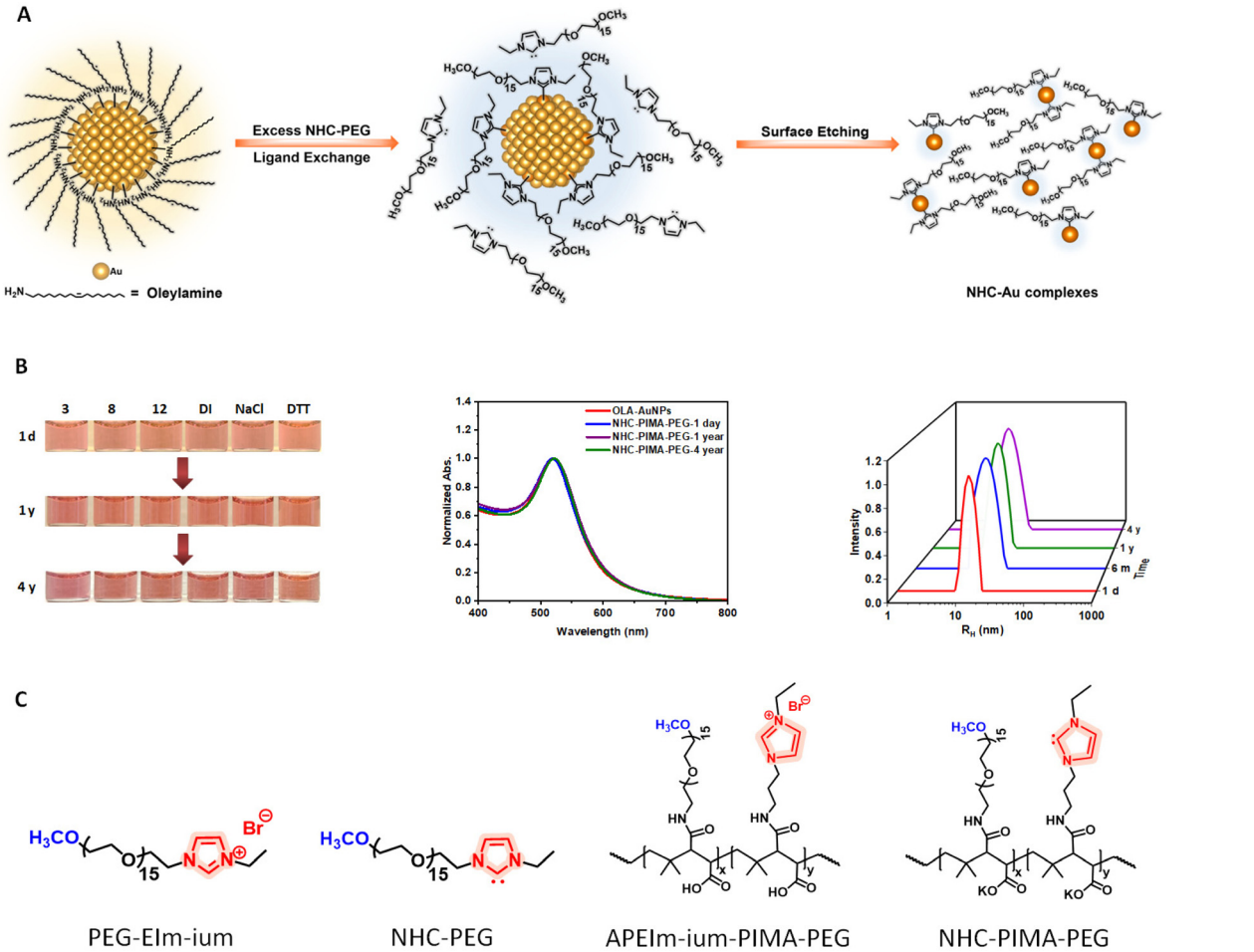

Fig. 1 (A) Schematic representation of the proposed transformation in which large excess of *in situ* generated NHC-PEG ligands (with respect to AuNPs) trigger a progressive etching of surface atoms. This ultimately yields monoNHC- and bisNHC–Au complexes freely diffusing in the medium. The generated NHC-PEG-complexed Au atoms are shown in orange. (B, left) White light images of several dispersions of AuNP stabilized with NHC-PIMA-PEG polymers in water media detailed in the figure and tracked over a 4-year period. (B, middle) UV-vis absorption spectra acquired from the dispersions shown in the left period. (B, right) Intensity *vs.* hydrodynamic radius measured using DLS showing only a single peak, indicating the presence of homogenous dispersions free of aggregation in all samples. (C, left) chemical structures of the monomer PEG-EIm-ium (precursor) and the PEG-NHC. (C, right) chemical structure of the APEIm-ium-PIMA-PEG precursor side-by-side with the NHC-PIMA-PEG used to collect the data in panel B. Additional details are provided in the ESI.†

or simplified as:

$$4Au(0) + 8CN^- + O_2 + 2H_2O \rightarrow 4[Au(CN)_2^-] + 4OH^- \quad (1b)$$

Accordingly, we reasoned that if coordination interactions between NHC-PEG and surface Au atoms compete with the Au-to-Au covalent interactions in a nanocrystal, a similar "digestion test" could be envisioned. Here, NHC-PEG ligands progressively complex with Au(I)-rich NP surfaces and competitively dislodge them, ultimately rearranging the NP structure. This leads to etching of the colloids, loss of the SPR signature, ultimately yielding soluble PEG-NHC-Au complexes. Key requirement for the experiment is the use of excess NHC-PEG (monomer) ligands, which essentially entails the implementation of ligand substitution but without including a routine purification step to remove excess ligands from the dispersion. The use of monomer instead of polymer NHC ligands enhances the process because of the higher desorption rates combined with higher Brownian dynamics of the smaller monomer ligands compared to their polymeric counterparts.

AuNP etching experiments

The core etching experiments were carried out using primarily the monoNHC-PEG ligands starting with as-grown OLA-AuNPs under hydrophobic conditions. The AuNPs were prepared using high-temperature growth reaction following literature protocols (see Experimental section).[60,61] Then, excess free OLA in the hexane stock dispersions was first removed by precipitation using excess ethanol then centrifugation at 3500 rpm for ~5–10 min. The supernatant was discarded and the resulting pellet was re-dispersed in tetrahydrofuran (THF). In a typical digestion experiment, four separate OLA-AuNP dispersions were first prepared. Each AuNP dispersion was mixed

with an excess molar amount of PEG-EIm-ium (also in THF); [PEG-EIm-ium] : [AuNPs] molar ratios of ~100 000 : 1, ~300 000 : 1, ~500 000 : 1 and ~700 000 : 1 were used. Then, a solution of KO*t*Bu dissolved in THF was added to each dispersion to promote the *in situ* carbene generation. The reaction mixture in each vial was left to progress at room temperature while stirring. The experiments were carried out using a fixed molar amount of KO*t*Bu that is 3-fold larger than the starting PEG-imidazolium, which guarantees efficient deprotonation of the C_2 protons in the sample. This value was chosen following a few preliminary test incubation experiments using several molar amounts of KO*t*Bu. Those experiments showed that excess amount of base with respect to ligand accelerates the core etching process (see ESI, Fig. S1†). They also showed that turbidity builds up in the sample when the base exceeds 30-fold excess. This can be attributed to aggregation of higher concentration KBr salt formed after reaction of Br^- anions with the base; note that the amount of KBr is determined by the molar concentration of imidazolium bromide in the sample. Such turbidity interferes with our ability to acquire absorption data. We chose 3-fold excess of base for all our measurements. We also note that deprotonation of the C_2 in the presence of added KO*t*Bu is rapid, requiring only few min (~2–4 min) of incubation.

We found that incubation using the above conditions triggers etching of the nanoparticles, which yields a progressive color change from pinkish/red to yellow solution with time. The rate of color change with time is controlled by the starting PEG-EIm-ium molar excess, with faster progression measured for higher ligand concentrations. Progression of NP etching for each sample was then tracked by monitoring changes in the absorption profile with time.

Post reaction characterization of the end product was carried out using 1D and 2D NMR spectroscopy, MALDI mass spectrometry and TEM measurements. The samples were subjected to one round of precipitation and centrifugation to remove the native displaced OLA ligands. Briefly, excess hexane was added to the sample after the incubation period is complete, followed by centrifugal precipitation and discarding the supernatant; this step removes the displaced OLA. For NMR sample preparation, one additional round of concentration/dilution was applied using a membrane filtration device with either a cutoff MW = 100 kDa (for AuNP dispersions not used for etching), or with cutoff MW = 10 kDa (for etched samples).[62] Additional details are provided in the ESI.†

Characterization of the NHC coordination interactions with gold nanoparticles

NMR characterization. Fig. 2A and B shows representative ^{1}H NMR spectra collected from a solution of pure PEG-EIm-ium salt (precursor to the NHC-PEG ligand) side-by-side with the one acquired from a dispersion of NHC-PEG-ligated AuNPs once the digestion reaction is complete (end of the incubation experiment); a [PEG-EIm-ium] : [AuNP] molar ratio of ~300 000 : 1 was used. The NMR samples were prepared in deuterium oxide (D_2O). The spectrum collected from PEG-EIm-ium (Fig. 2A) shows a few key characteristic peaks: one merged signal at 7.56 and one single signal at 8.84 ppm respectively assigned to the $C_{4,5}$ and C_2 protons in the heterocyclic ring, along with two signals at 4.41, 3.93 ppm attributed to the C_8 and C_9 protons attached to N_3 and a signal at 4.27 ppm ascribed to the C_6 protons in the methylene attached to N_1. Conversely, the spectrum in Fig. 2B, acquired from PEG-NHC-AuNPs after digestion, shows a new upfield signature (at 7.36 ppm) compared to the same protons in the PEG-EIm-ium precursor (at 7.56 ppm), which is assigned to the merged signal of imidazolium backbone protons (*i.e.*, $C_{4'5'}$) following coordination of the NHC moieties onto Au surfaces, attributed to the electron donating property of the ligands (strong sigma donor and weak pi acceptor). More precisely, the PEG-EIm-ium is positively charged and thus electron deficient. It deshields the imidazolium protons (4,5) and yields a downfield signature (at 7.56 ppm). Conversely, the configuration of the neutral NHC in the monoNHC–Au(I) is more electron-rich, which shields the protons (4′,5′) and upfield shifts its signature (at 7.36 ppm). Additionally, signatures of the protons attached to the N_3 and N_1, are slightly shifted downfield to 4.46 (C_8'), 4.30 (C_6') and 4.01 (C_9') ppm compared to those measured for the imidazolium salt. A close analysis of the NMR profile collected from the sample following digestion, in particular the integration values of the signals between 3.8 and 4.4 ppm, indicates that the sample contains a mixture of PEG-EIm-ium precursor, monoNHC–Au, as well as bisNHC–Au. More precisely, the signatures at 3.93 ppm (9 and 9″), at 4.26 ppm (6 and 6″) and at 4.42 ppm (8 and 8″), all with an integration of 6 protons, emanate from precursor and bisNHC–Au. This is also consistent with the signal at 1.52 ppm (7_x = 7, 7′ and 7″) having an integration of 12 protons, which include contributions of all three species: precursor, monoNHC–Au, and bisNHC–Au (see data in panel **2B**). The signatures at 3.72 ppm (10_x) and at 3.40 ppm (11_x) also account for the presence of three species. We also note that the signature of the backbone protons in the bisNHC–Au (4″ and 5″) has shifted back downfield to 7.56 ppm compared to the one measured for monoNHC–Au above (at 7.36 ppm). Here, the presence of two NHC ligands coordinated onto the gold(I) center produce electron distribution over the two heterocycle rings (stronger pi back bonding), and resulting in a downfield shift to 7.56 ppm.

Remark-1: *It should be noted that a very weak signature ascribed to the C_2 acidic proton can be detected at 8.84 ppm in panel B. This may indicate protonation of a small fraction of carbene moieties (due to the moisture sensitive nature of NHC), which could occur during sample purification and transfer to D_2O. This amount can also be affected by potential proton to deuterium substitution, nonetheless.*

1D ^{13}C NMR and 2D ^{13}C–^{1}H HMBC NMR measurements have been applied to gain additional evidence about the Au–carbene bond. It has been reported that upon carbene generation the ^{13}C NMR signature of the C_2 atom of free NHCs experiences a significant downfield chemical shift to ~200 and 250 ppm, while that signature can be measured between 130

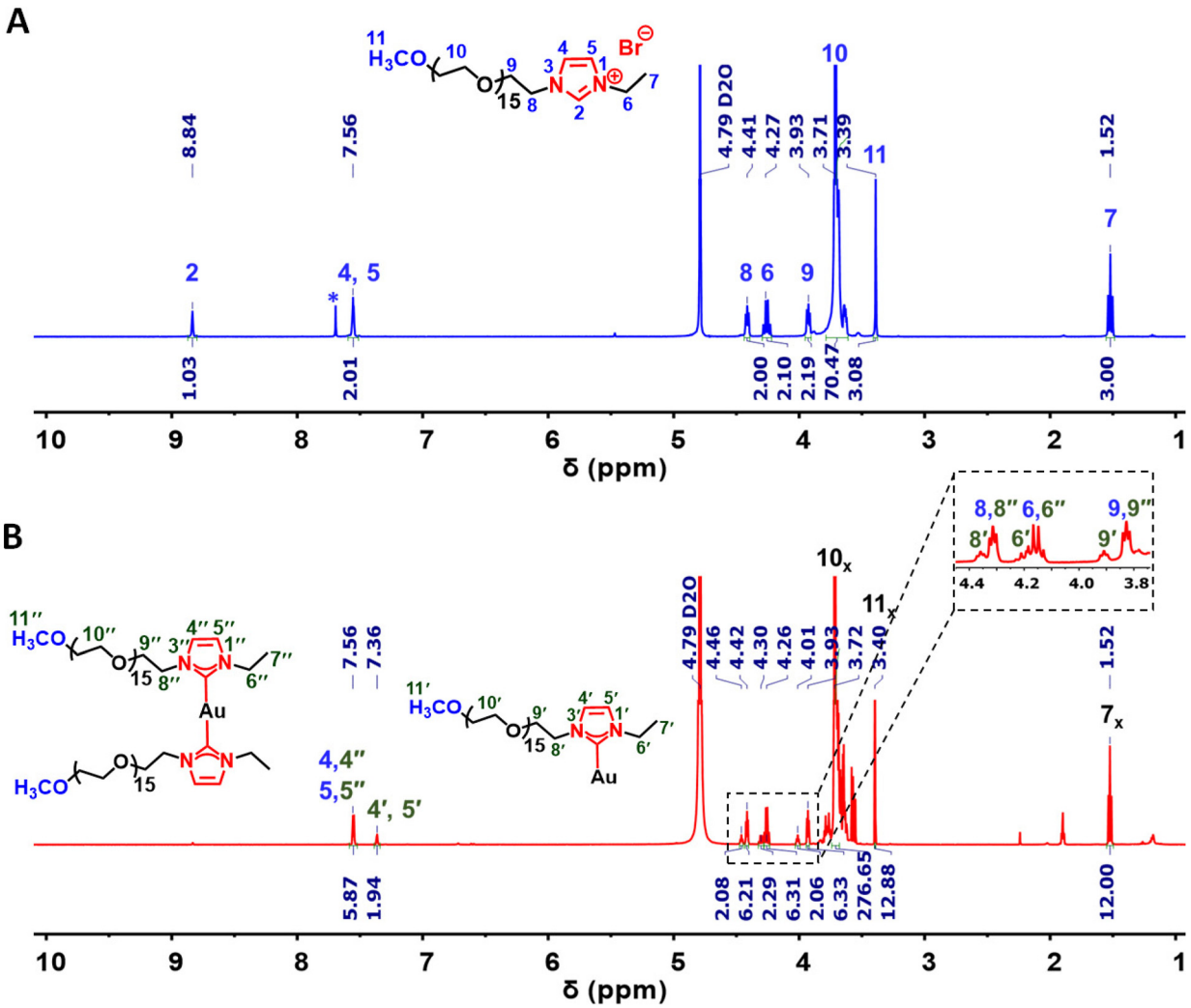

Fig. 2 ^{1}H NMR spectra acquired from: (A) PEG-EIm-ium salt precursor; (B) the PEG-NHC-Au complexes formed following extended incubation of AuNPs with large excess of monomer NHC-PEG. Assignment of key protons in the ligands and ligand–Au complexes was confirmed using peak integration values. All samples used in this study were prepared in D_2O and a [PEG-EIm-ium] : [AuNPs] molar ratio of ~300 000 : 1 was used.

and 160 ppm for the corresponding imidazolium salt.[63,64] However, once NHC is coordinated to a metal center, following complexation, the signature of the carbene carbon is shifted downfield.[65–67] Fig. 3A and B shows representative 1D ^{13}C NMR spectra collected from solutions of the PEG-EIm-ium precursor side-by-side with the corresponding surface-digested PEG-NHC-Au dispersed in dimethyl sulfoxide-d_6 (DMSO-d_6). The spectrum acquired from PEG-EIm-ium shows three distinct signals: located at 136.0, 122.7 and 121.8 ppm which are ascribed to the C_2, C_4 and C_5 carbons, respectively. The ^{13}C NMR spectrum measured for the PEG-NHC-Au (etched sample) presents a new downfield resonance corresponding to the metallated carbene carbon atom at 182.2 ppm, in addition to the three signals discussed above for the PEG-EIm-ium precursor. These data combined provide strong evidence that NHC-to-metal complexation has indeed taken place.

2D HMBC NMR spectra were also acquired from the sample following incubation to confirm that NHC-to-Au complexation has taken place. HMBC experiments are often employed to enhance the ^{13}C signature through correlation between a given target carbon and protons that are few bonds away.[68,69] Indeed, the HMBC spectrum acquired from our sample shows that all cross signals of the ethylene glycol and terminal methyl carbons at 67.8 (C_{11}) and 69.6 ppm (C_{10}) and their corresponding protons at 3.40 and 3.72 ppm (H_{11} and H_{10}) are observed (see Fig. 3C and Fig. S2†). Though providing strong signatures, that region of the spectrum will not be further exploited, given the fact that a large number of protons is present along the PEG chain. Instead, we focus on the additional cross signatures emanating from ethyl group at N_1 and methylene group at N_3 which are observed over the 4.25–7.5 ppm range. We expand the downfield chemical shift region where NHC complexation to Au surface is expected to produce a signature in the ^{13}C NMR profile, see Fig. 3D. Indeed, the 2D spectrum shows three cross peaks. The first and second signals designate the correlation between the

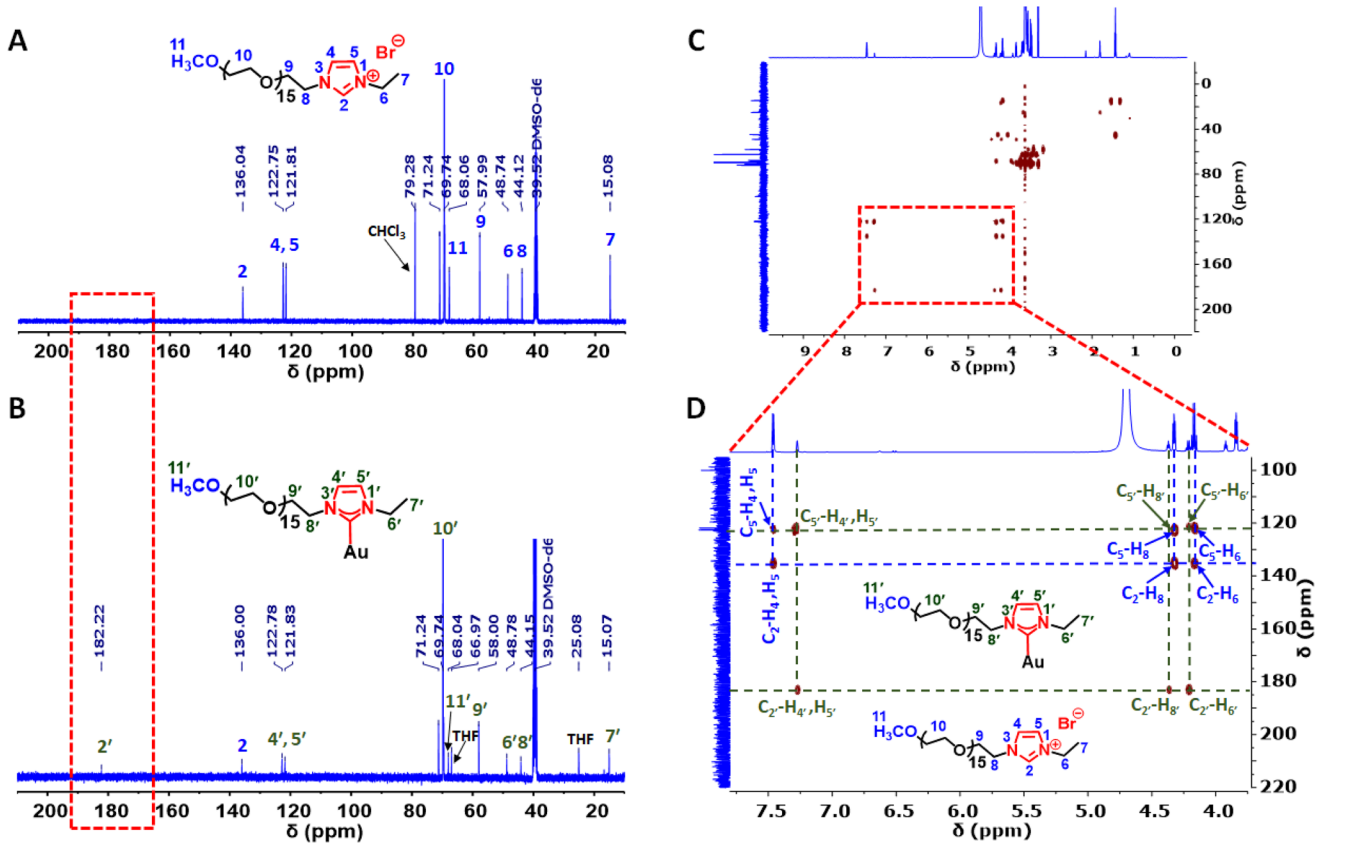

Fig. 3 Stacked 1D ^{13}C NMR spectra acquired from: (A) a solution of the PEG-EIm-ium salt precursor; (B) PEG-NHC-Au etched dispersion. The signal at ~182.2 ppm is ascribed to the carbene carbon (C_2). All samples were prepared in DMSO-d_6. (C) 2D ^{1}H and ^{13}C HMBC spectrum correlating specific ^{1}H and ^{13}C signatures around the imidazole ring for the PEG-NHC-Au complexes formed during NP etching using excess NHC-PEG. (D) Expansion of HMBC spectrum shown in (C) focusing on the 100–220 ppm range. The 2D ^{1}H and ^{13}C HMBC spectrum was collected in D_2O. All measurements were carried out using ~300 000 : 1 [PEG-EIm-ium] : [AuNPs] molar ratio.

carbene carbon at 183.2 ppm and the protons at 4.3(H_6') and 4.46 (H_8') ppm of the methylene groups at N_3 and N_1, respectively. The third measured cross signature correlates the same C_2 carbon at 183.2 ppm with protons at 7.36 ppm (H_4', H_5') in the heterocyclic ring backbone. Note that the position of the C_2 signal measured here differs slightly from that measured above because two different solvents (DMSO-d_6 *vs.* D_2O) were used. These results are indicative of the existence of NHCs as the coordinating motifs on the Au surface. Moreover, the observed chemical shift of our PEG-NHC-Au complexes are in good agreement with literature values for other NHC–Au complexes.[70–72] We note that the signatures shown at 1.52 (H_7') and at 4.01 ppm (H_9') do not show cross-correlation with the C_2 center in the 2D spectrum, which can be attributed to the fact that they are positioned three bonds farther from the carbene center.

Mass spectrometry data. Fig. 4A and B shows the MALDI-TOF mass spectra acquired from the PEG-EIm-ium salt precursor side-by-side with that measured for the etched sample containing NHC–Au complexes. The spectrum collected from the ligand only features one broad Gaussian peak centered at 815 Da that corresponds to the calculated mass of PEG-EIm-ium ligand without bromide counterion; the broad mass distribution is attributed to the polydisperse nature of the PEG moieties, where a set of narrow peaks separated by the mass of the repeat ethylene glycol units (44 Da) that are superposed on the top of the main one (see Fig. 4A). The spectrum measured from the NHC–Au digested sample shows three main peaks centered at approx. 815, 1011 and 1782 Da, each showing the characteristic PEG set of narrow peaks separated by 44 Da corresponding to the PEG block (see Fig. 4B). Fig. 4, panel **B** shows that in addition to the PEG-EIm-ium peak at ~815 Da, there are two broad peaks one weak corresponding to the mass of monoNHC–Au complex (at ~1011 Da) and a stronger one (at 1782 Da) ascribed to mass of bisNHC–Au complex. Overall, the MALDI results are consistent with the data collected from the ^{1}H NMR experiments (Fig. 2). The larger mass peak of bisNHC–Au complexes can be attributed to the rather large molar concentration of ligands (compared to Au atoms) in the medium, which favors the formation of Au-complexes with two NHC-PEG, see Table 1.[51]

TEM data. High-angle-annular-dark-field scanning transmission electron microscopy (HAADF-STEM) was applied to gain additional information about core size and morphology

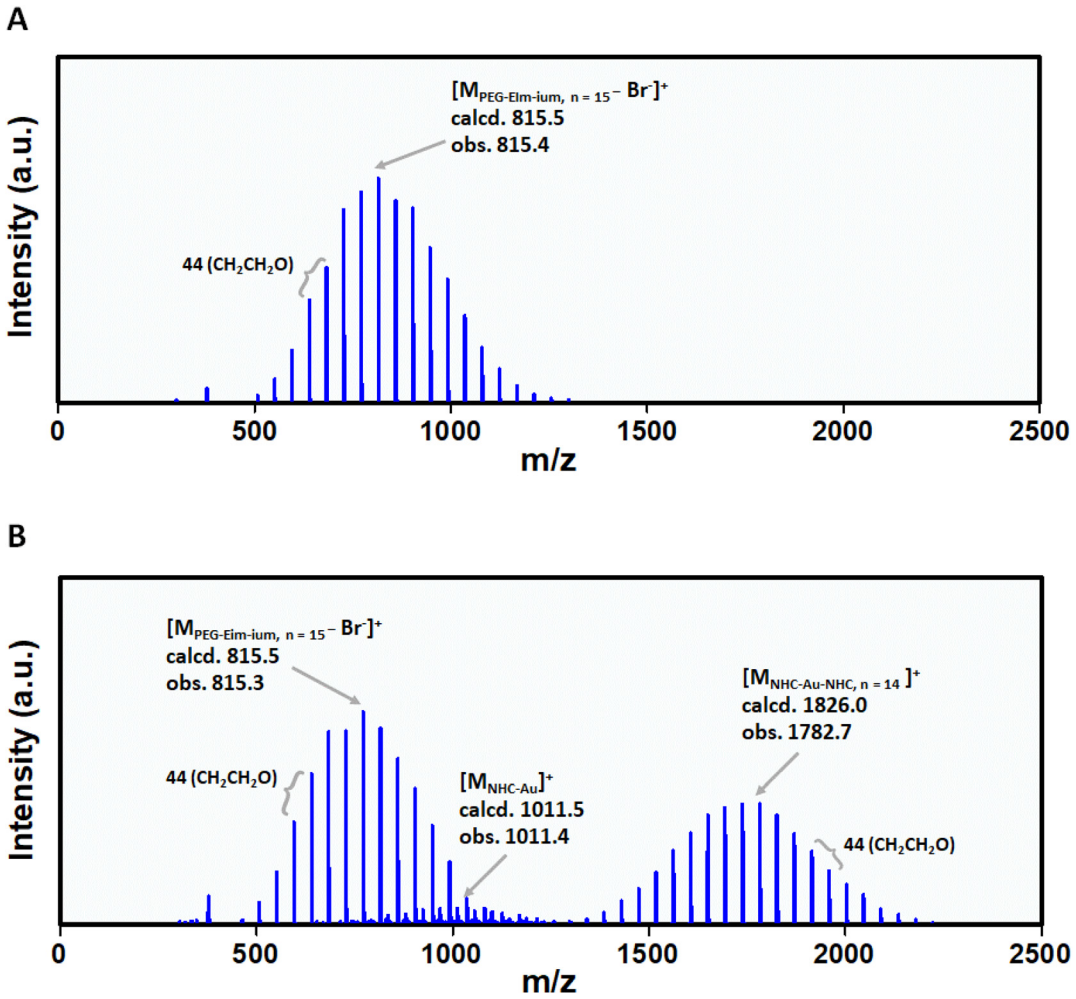

Fig. 4 (A and B) MALDI mass spectra measured for the PEG-Elm-ium salt precursor (A) and for the PEG-NHC–Au complexes formed as product of NP etching (B).

Table 1 Parameters relevant to the NHC-PEG-induced etching of the AuNPs, including NP and ligand concentrations, numbers of total and surface Au atoms per nanoparticle, along with the digestion time (t_D) extracted from fits to the data

Fold excess ligands[a]	N_{S-Au}[b]/NP	N_{T-Au}[c]/NP	[AuNP][d] (M)	[NHC-PEG][e] (M)	NHC-PEG/N_{S-Au} ratio	NHC-PEG/N_{T-Au} ratio	t_D (min)
100 000	4412	$\sim 3.08 \times 10^4$	5.6×10^{-9}	0.56×10^{-3}	23	3	600
303 571	4412	$\sim 3.08 \times 10^4$	5.6×10^{-9}	1.7×10^{-3}	69	10	469
500 000	4412	$\sim 3.08 \times 10^4$	5.6×10^{-9}	2.8×10^{-3}	113	16	283
714 285	4412	$\sim 3.08 \times 10^4$	5.6×10^{-9}	4.0×10^{-3}	162	23	64

[a] Equal to [NHC-PEG]/[OLA-AuNPs]. [b] N_{S-Au} is the number of surface Au atoms per NP. [c] N_{T-Au} designates the total number Au atoms per NP. [d] [AuNP] is the AuNP molar concentration. [e] [NHC-PEG] is the molar concentration of ligand.

of gold nanocrystals before and after digestion experiments, using NHC-PEG (Fig. 5). The as-prepared OLA-AuNPs have a spherical shape, with an average diameter of ~10 nm and exhibit the usual SPR peak at 520 nm (see Fig. 5A, C and E). In comparison, the UV-vis spectrum acquired from the clear yellowish solution obtained following incubation with the NHC-PEG ligands indicates that the SPR feature has completely disappeared (Fig. 5B). TEM characterization of the materials present in the yellowish solution did not yield any NPs but a very few nanoclusters with diameter of 0.6 nm; these do not show the crystalline arrangements of atoms usually observed for nanoparticles (diameter > 2 nm) (see circled objects in panels **D** and **F**).[62] Formation of these small size AuNCs can be attributed to aurophilic interactions between NHC–Au(I) complexes.[73–75] Overall, the TEM data confirm that incubation with NHC-PEG results in the disappearance of AuNPs, which agrees with the UV-vis absorption and Mass Spectrometry data. TEM cannot resolve individual PEG-NHC-Au complexes.

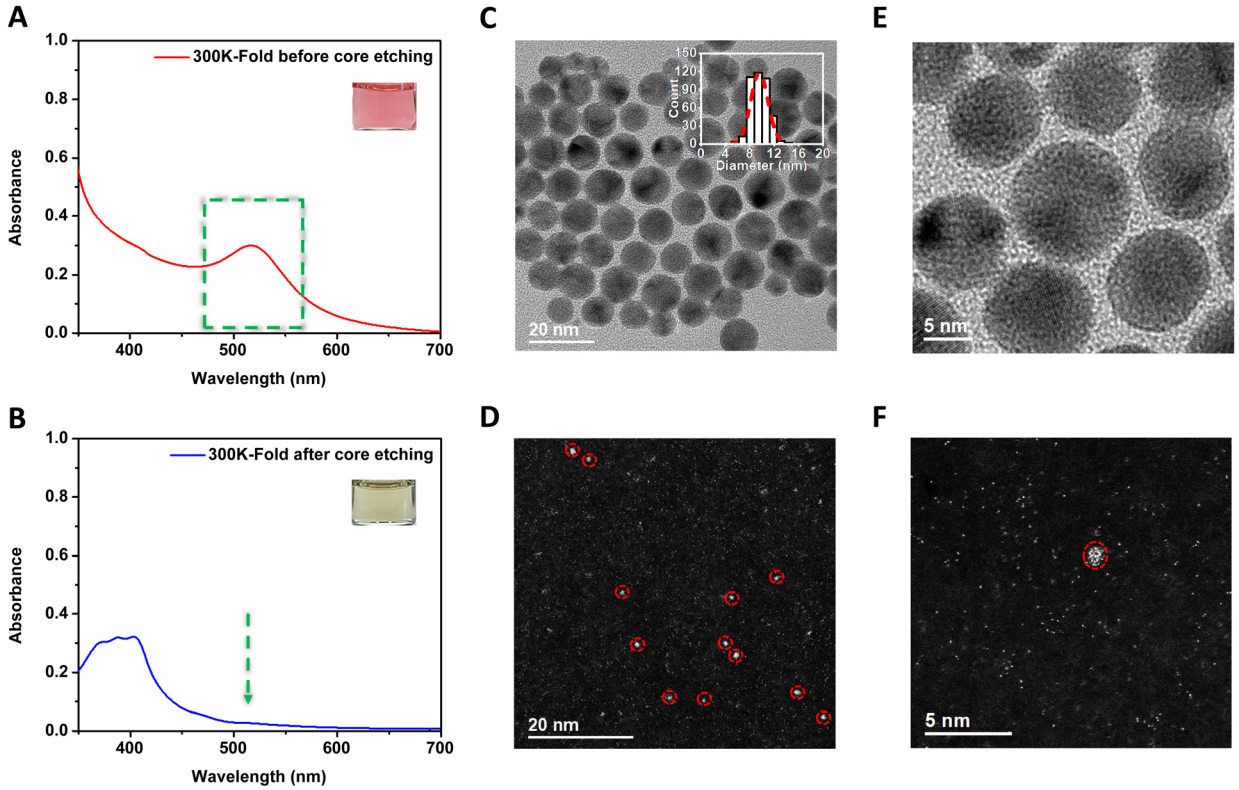

Fig. 5 (A and B) Side-by-side UV–vis spectra collected from a dispersion of OLA-AuNPs mixed with PEG-EIm-ium salt (at molar excess with respect to the NPs, red curve) before and after the introduction of base. A well-defined SPR at 520 nm is shown in panel A. The insets in panels A and B show white light images of dispersions before and after etching. The profile in panel B shows no SPR signature, indicating NP digestion (blue curve). (C and E) Different magnification TEM images acquired from OLA-AuNPs. A size distribution histogram of OLA-AuNPs is shown in panel C; average diameter ~9.6 ± 1.4 nm is deduced. (D and F) Different magnification images of materials collected after extended incubation of the AuNPs with excess NHC-PEG. Only a few nanoclusters can be identified. UV-vis spectra and TEM images were collected using ~300 000-fold excess ligands.

Remark-2: *The above experiments relied on the use of a strong base for the carbene generation. We synthesized a different complex, PEG-NHC-Au-Cl, as control NHC-complex, through reaction of Me_2S–Au–Cl with the PEG-EIm-ium in the presence of K_2CO_3 (a weak base) at 60 °C for 5 h. In this approach, which we refer to as "weak base route" reaction between the metal precursor and azolium salt in the presence of a weak base (e.g. NaOAc, K_2CO_3 or NEt_3) triggers the in situ carbene generation and allows for one-step synthesis of the corresponding metal–NHC complexes.*[12,76] *The PEG-NHC-Au-Cl complex exhibits negligible absorption at the SPR signature (see ESI, Fig. S3†), which agrees with the absorption profile measured for the etched samples using KOtBu. The NMR data shown in Fig. S3† account for all the protons in the above complex. Nonetheless, a direct comparison of the proton signatures to those measured in the digested sample (shown in Fig. 2) could not be carried out because two different deuterated solvents were used for the control and digested samples.*

Digestion kinetics

The data shown above prove that extended interactions of AuNPs with a large excess of NHC-PEG promotes top-down etching of the nanocrystals. Furthermore, the time required for complete digestion strongly depends on the ligand molar excess used. This has motivated us to devise one additional experiment to assess the kinetics of the NP etching by drawing a comparison to the more classical NaCN-induced digestion of metal nanostructures and, in a more general industrial framework, the isolation of pure metals from their ores. It has been shown that when gold ore is mixed with NaCN salt, gold ions are extracted in the form of gold-cyanide complexes, as shown in the chemical equations (1a) and (1b).[77] Indeed, NaCN-induced digestion test has been used by a few groups, including ours, in the field of surface chemistry to evaluate the effects of a particular surface coating strategy to shield the metallic cores from the surrounding CN anions and maintain the colloidal stability of several Au nanocolloids with varying shape and morphology.[56,59,78,79]

Here, we apply the same analytical approach where we assess the ability of NHC-PEG ligands, added in molar excess, to kinetically digest AuNPs by tracking the progressive change in the absorption profile until complete loss of the SPR feature. Experimentally, we assume that when NHC moieties tightly coordinate onto AuNPs they progressively dislodge the surface atoms one by one and form freely diffusing PEG-NHC-Au complexes. This process converts the reddish

color of the AuNPs dispersion into a yellowish solution, which manifests in a time-dependent reduction of the SPR peak.

We tracked the time-progression of the UV-vis absorption spectra collected from dispersions of AuNPs (with [AuNP] = 5.6 nM) that have been incubated with excess NHC-PEG under the conditions tested above, namely, [NHC-PEG] : [AuNP] ~100 000 : 1, ~300 000 : 1, ~500 000 : 1 and ~700 000 : 1 (see Table 1). For each sample, the first absorption spectrum was recorded immediately after the addition of KO*t*Bu (~2 min). Then, additional absorption spectra were collected at blocks of 15 min, 30 min and 1 h intervals (depending on how fast the changes occur) until the sample color becomes yellowish clear. The data in Fig. 6A–D show that there is a progressive decrease in the absorption spectrum with time for all samples. Specifically, faster decay in the SPR peak with time was observed for 700 000-fold molar excess NHC-PEG compared with the 300 000- and 500 000-fold excess, indicating faster digestion for higher ligand concentrations. Progression of the SPR absorbance *vs.* time was fitted to an exponential decay function:[56,59]

$$A_{520} = A_0 e^{-t/t_D} \quad (2)$$

where A_0 is the initial absorbance value at t = 0 min and t_D refers to a digestion time. Alternatively, a linear fit to the SPR data using ln(A) *vs.* t can be used, see Fig. S4.† We note that because a large excess of ligand concentration is used compared to that of the AuNPs, we ascribe a pseudo-first order kinetics to the digestion reaction. The data summarized in Fig. 6E–H show that the digestion time tracks the molar ligand excess, with t_D = 600 min for 100 000-fold excess, t_D = 469 min for 300 000-fold excess, t_D = 283 min for 500 000-fold excess, and t_D = 64 min for 700 000-fold excess. Table 1 shows a summary of the conditions used for the 10 nm NP digestion measurements. A simple plot of t_D *vs.* molar excess ratio yields a linear decay curve, confirming that the rate of etching/digestion follows a pseudo first order reaction kinetics (see Fig. S4†). We should note that the NP transformation cannot be promoted by the rather large excess of base used (to match the high molar concentrations of the ligands). Control experiments evaluating the effects of incubating AuNPs with KO*t*Bu showed that complexation of potassium ions with OLA produces turbidity in the solution along with absorption in the UV region of the absorption spectrum. The NP integrity is not lost, see Fig. S5.†

We would like to stress that the observed AuNP etching following incubation with excess NHC-PEG is also observed when AuNPs are incubated with the NHC-polymer (NHC-PIMA-PEG) instead; the polymer presents ~20 NHC groups per chain.[27,29] The molar excess of NHC-polymer was adjusted to account for the fact that a single chain presents several NHCs per macromolecule. However, the etching kinetics are substantially slower than those measured above. For example, while using a 700 000-fold mono-NHC produces a complete loss of SPR after ~500 min, such process requires incubation exceeding 4000 min when NHC-PIMA-PEG is used (see Fig. S6†).

We also carried similar incubation of OLA-AuNP dispersions with large excess of two thiol-presenting ligands, to establish a comparison between the etching kinetics triggered by the two types of anchors. Reported estimates for the coordination bond energy for various Lewis base groups indicate that the bond energy for Au–S is smaller than Au–NHC, which would lead to assume that incubation of AuNPs with thiol-modified molecules could induce etching, but the kinetics of this process would be much slower. To test this hypothesis, we monitored the progression of the UV-vis absorption profile for the AuNPs coated with two sets of thiol-appended ligands: (1) AuNPs incubated with excess SH-PEG (a monothiol-appended PEG).[62] The molar excesses of this ligand was comparable to that of NHC-PEG. (2) AuNPs coated with lipoic acid-appended PEG ligand (LA-PEG); we used the same methoxy-terminated PEG_{750}-OCH_3 motif to prepare all three LA-PEG, SH-PEG and NHC-PEG. The chemical structures of these ligands are provided in the ESI, Fig. S7.† We adjusted the molar concentration of LA-PEG to half that of SH-PEG in order to account for the higher thiol coordination expected for the reduced lipoic acid compared to the monoNHC and monothiol ligands. Ligand substitution of OLA-AuNPs with LA-PEG was implemented using *in situ* photoligation using a laboratory photoreactor providing a 100 nm UV band centered at 350 nm and a power of 4.5 mW cm^{-2} (Model LZC-4 V, Luzchem Research, Inc., Ottawa, Canada).[59,80] Conversely, conventional incubation was used for ligand exchange with SH-PEG ligands. UV-vis spectra were measured at fixed intervals for several hours as done above. Results from both sets of measurements indicate that core etching using thiol-appended ligands can be measured but the kinetics are substantially slower than what measured for NHC-PEG. More precisely, a complete loss of the pink/reddish color does not happen even after 12 days of incubation with LA for any ligand excess used (see Fig. 7). Similarly, incubation with mono-thiol PEG produces a slightly faster rate of etching, but the t_D values measured for both ligands are ~one order of magnitude slower than those measured for NHC-PEG. Tables 2 and 3 summarize the conditions and t_D values measured for the incubation using large excesses of dithiol-PEG or monothiol-PEG ligands. We note that digestion of other metal core nanocrystals, namely, AgNPs using excess thiol-molecules in acidic conditions (using added HCl) have been reported.[81] Additionally, literature reports have employed etching of larger size AuNPs using excess thiol-containing molecules (*e.g.*, glutathione) or polyethylenimine to prepare fluorescent Au nanoclusters.[75,82,83]

We now compare the formation of the NHC–Au complexes triggered by incubation of OLA-AuNPs with molar excess of NHC-PEG to previous experimental and theoretical studies.[4,51] Our findings are in agreement with data reported by Richeter and coworkers, who investigated the reactivity of AuNPs towards NHC ligands and showed formation of biscarbene–Au (I) complexes in their AuNP samples.[51,52] A proposed mechanism to interpret the formation of NHC–Au(I) complexes and NHC-grafted AuNPs involves the following steps: initially, weakly adsorbed surface ligands are substituted with NHC

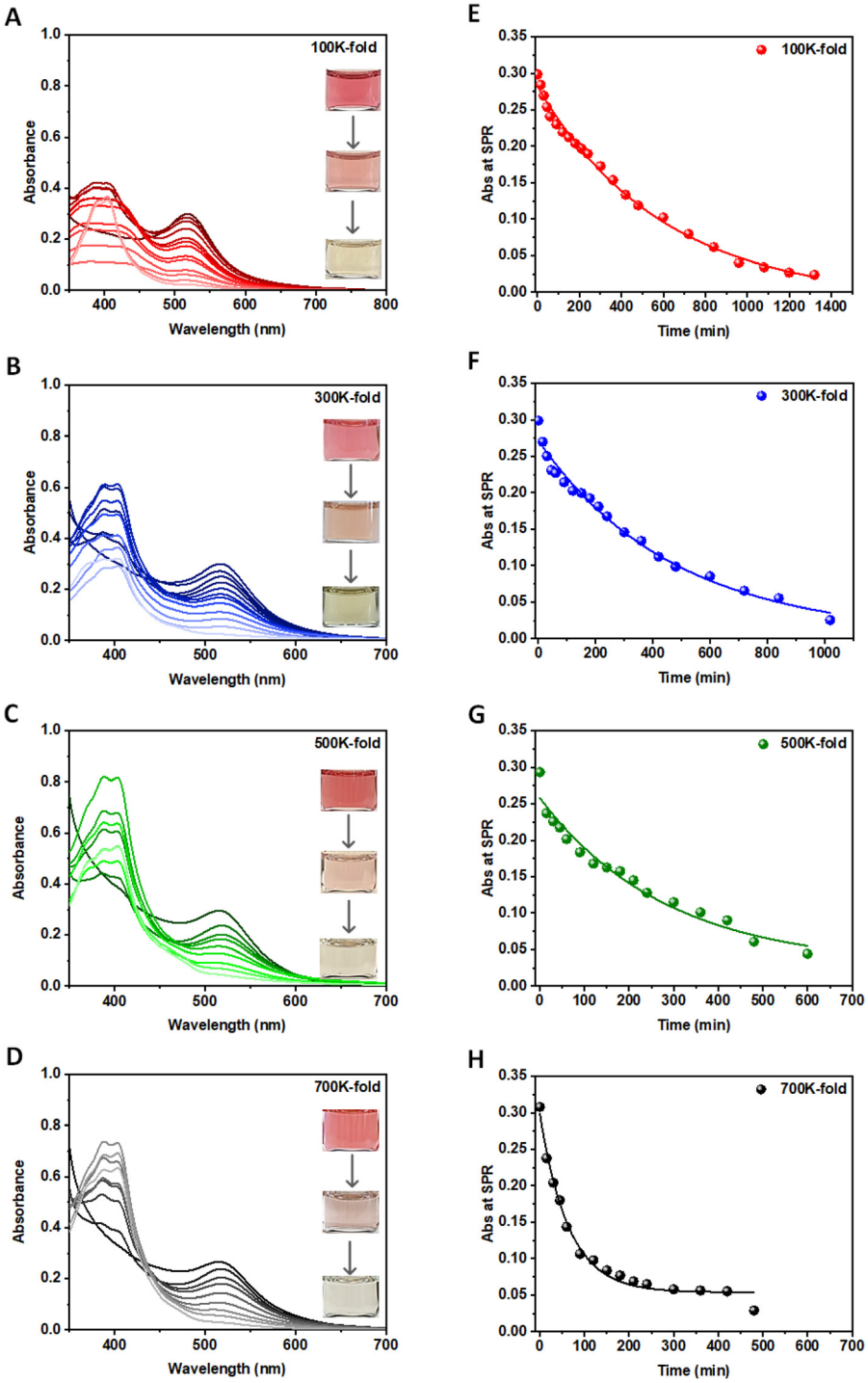

Fig. 6 Time-progression of absorption spectra collected from as grown AuNP dispersions incubated with four different molar concentrations of NHC-PEG ligands (*in situ* generated) in excess. Molar ratios of ligand : AuNP used are (A) ~100 000 : 1, (B) ~300 000 : 1; (C) ~500 000 : 1; (D) ~700 000 : 1. Insets are white light images of the dispersions showing progressive color change of Au colloids with time during NHC-PEG-induced etching. (E–H) Time-dependent progression of the SPR peak value was extracted from the four sets of data shown in panels A–D.

molecules. Then, due to their high binding energy onto AuNPs surfaces, NHC moieties dislodge Au atoms from the surface (as Au(I)), causing reorganization of the underlying gold lattice by forming surface defects such as NHC–Au(I) adatom complexes. Subsequently, the released NHC–Au species further react with the remaining free NHC ligands in the dispersion, leading to the formation of biscarbene–Au(I) complexes. This is consistent with our mass spectrometry data shown in Fig. 4. This rationale is also consistent with results reported by Chechik's and Fuchs's groups, where they showed that ligation

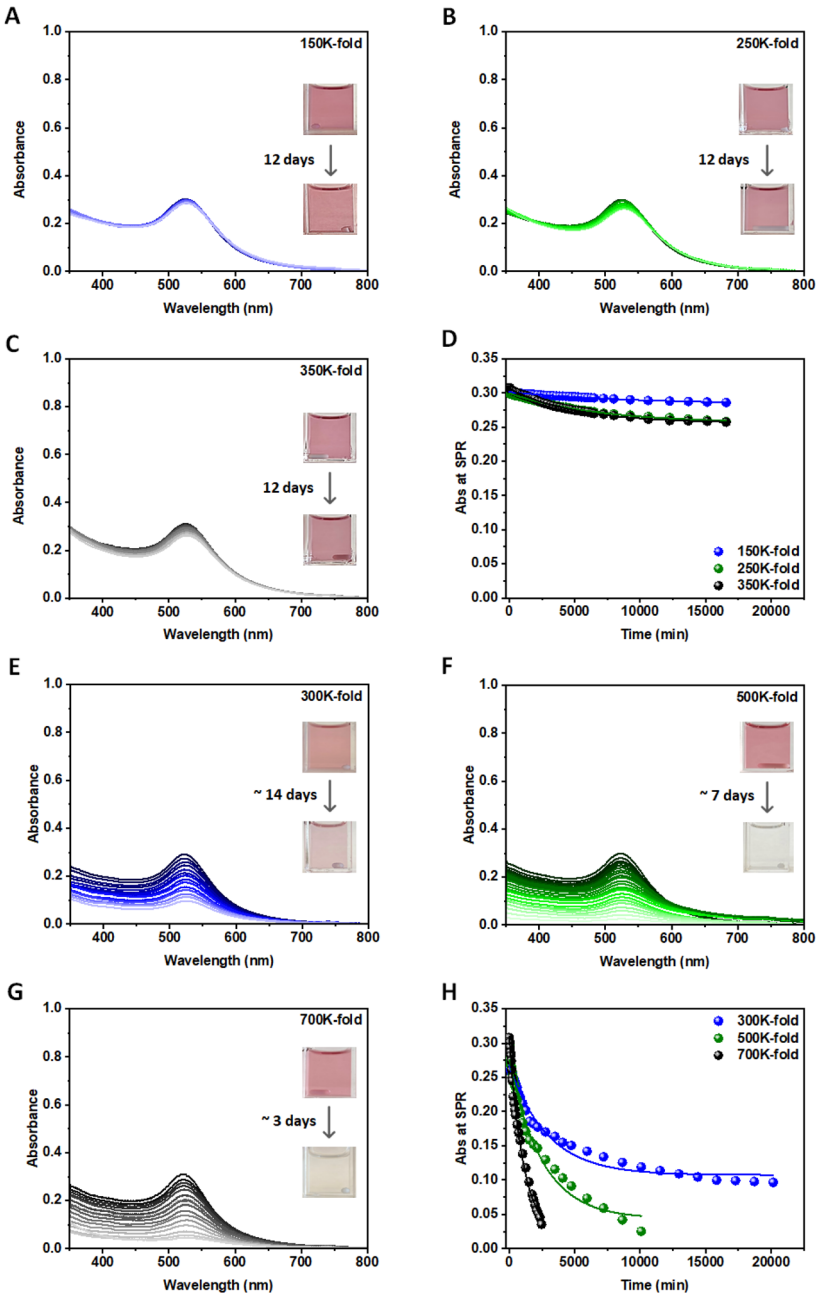

Fig. 7 Time-progression of the UV-vis absorption spectra collected from AuNP dispersions incubated with three molar amounts of LA-PEG or SH-PEG. Panels (A–C) show data acquired for dispersions mixed with LA-PEG and photo-irradiated with a UV signal to promote rapid ligand substitution of OLA-AuNPs; the molar ratio of LA-PEG-to-AuNPs was: (A) ~150 000 : 1; (B) ~250 000 : 1; (C) ~350 000 : 1. (D) Compiled data showing the progress of A_{520} *vs.* time from spectra in A–C. (E–G) UV-vis absorption spectra collected from AuNP dispersions incubated with three molar amounts of SH-PEG ligands. The molar excess of SH-PEG *vs.* AuNPs was: (E) ~300 000 : 1; (F) ~500 000 : 1; (G) ~700 000 : 1. (H) Compiled data for the progress of A_{520} *vs.* time from spectra shown in E–G. Insets in the various panels show white light images of the AuNPs at the start and end of the incubation period.

Table 2 Parameters used in the ligand-induced etching in the presence of LA-PEG, as done in Table 1

Fold excess ligands[a]	N_{S-Au}[b]/NP	N_{T-Au}[c]/NP	[AuNP][d] (M)	[LA-PEG][e] (M)	LA-PEG/N_{S-Au} ratio	LA-PEG/N_{T-Au} ratio	t_D (min)
150 000	4412	$\sim 3.08 \times 10^4$	5.6×10^{-9}	0.84×10^{-3}	34	5	9700
250 000	4412	$\sim 3.08 \times 10^4$	5.6×10^{-9}	1.4×10^{-3}	57	8	6763
357 142	4412	$\sim 3.08 \times 10^4$	5.6×10^{-9}	2.0×10^{-3}	80	12	5100

[a] Equal to [LA-PEG]/[OLA-AuNPs]. [b] is the number of surface Au atoms per NP. [c] designates the total number Au atoms per NP. [d] [AuNP] is the AuNP molar concentration. [e] [LA-PEG] is the molar concentration of ligand.

Table 3 Parameters for the ligand-induced etching in the presence of monothiol-PEG, as done in Tables 1 and 2

Fold excess ligands[a]	N_{S-Au} [b]/NP	N_{T-Au} [c]/NP	[AuNP][d] (M)	[SH-PEG][e] (M)	SH-PEG/N_{S-Au} ratio	SH-PEG/N_{T-Au} ratio	t_D (min)
285 714	4412	$\sim 3.08 \times 10^4$	5.6×10^{-9}	1.6×10^{-3}	65	9	3027
500 000	4412	$\sim 3.08 \times 10^4$	5.6×10^{-9}	2.8×10^{-3}	113	16	2478
696 428	4412	$\sim 3.08 \times 10^4$	5.6×10^{-9}	3.9×10^{-3}	158	23	1093

[a] Equal to [SH-PEG]/[OLA-AuNPs]. [b] is the number of surface Au atoms per NP. [c] designates the total number Au atoms per NP. [d] [AuNP] is the AuNP molar concentration. [e] [SH-PEG] is the molar concentration of ligand.

of NHC molecules onto AuNPs and Au surfaces trigger leaching of NHC–Au(I) complexes into the surrounding medium.[53,54,84] In a subsequent report, Johnson and coworkers applied the 'adatom addition' strategy for the stabilization of gold nanorods in order to reduce/eliminate etching of the gold surfaces. For this, they designed a bidentate thiolate–NHC–Au(I) complexes then allowed the thiolate to graft onto the Au nanorod surfaces through ligand exchange. Subsequently, the NHC–Au(I) complex was installed on the surface as an adatom to prevent surface reconstruction.[26] These results support our observation that extended incubation with molar excess of NHC-PEG initiates surface lattice reorganization and etching of AuNP surfaces, leading to the formation of NHC–Au complexes and eventually digestion of the nanocrystals.

The discussed mechanism can also explain the slower digestion kinetics measured for the NPs reacted with NHC-PIMA-PEG polymer, where the much higher coordination affinity of the multidentate polymer onto the AuNPs, compared to the monoNHC molecules, makes dislodging individual atoms away from the NP surfaces much less frequent. Incubation of the AuNP dispersions with thiol-modified ligands provide weaker interactions with the NPs, which prevents the thiolates from competitively and efficiently dislodging ligand–Au(I) complexes, as reflected in the data shown above. Lastly, our rationale for developing a "parallel" between the strength of the coordination interactions of NHC moieties towards AuNP surfaces to the reaction of NaCN molecules with Au surfaces seems intuitive. When NHC/NaCN molecules come into contact with the AuNPs, they form complexes with the surface gold atoms. Cumulative removal of those complexes gradually etches the surfaces, resulting in digestion of the nanoparticles. This process as a whole occurs with higher frequency when using larger molar excess of the NHC-PEG. By fitting the time-dependent dampening of the SPR band to an exponential decay function, a decomposition rate is measured.[85] Though a chemical reaction similar to eqn (1a) and (1b) involving, for example oxidation, cannot be formulated, a coordination reaction between the NHC-PEG and Au(I) surface atoms triggers their dislodging, yielding NHC–Au(I) complexes that diffuse away from the nanocrystal. Reattachment is less likely as another free NHC-PEG will rapidly coordinate on the next layer of Au(I) atoms. Lattice reconstruction and formation of mono and bisNHC–Au complexes ultimately lead to etching of AuNPs manifesting in a time- and concentration-dependent loss of SPR features. The use of monomeric NHC (or thiol) ligands for the experiments allowed us to generate faster kinetics compared to higher coordination ligands. The faster kinetics observed for NHC ligands reflect stronger coordination binding on the NP surfaces than those governing covalent interactions between Au atoms.

Finally, we would like to provide a brief comparison between our etching results and those measured using different chemical reagents such as *N*-bromosuccinimide (NBS), IBr, *N*-halo succinimides and glutathione-plus-DNA.[86–89] The etching described in the above references is promoted by catalytic oxidation of Au surfaces which is triggered among others by halide radicals or a mixture of nucleic acid and glutathione. Etching using NBS, in particular, involves interactions with freed bromide radicals, which promotes catalytic oxidation of Au surfaces, leading to the formation of $(AuBr_4)^-$ complexes. The formed complex molecules are soluble Au(III) substrates and thus are different from those identified in our study. The etching promoted by NHC coordination involves dislodging of Au atoms triggered by the competitive NHC-to-Au binding, and is physically different from the one described in the above references. We note that if incubation was limited to ligand exchange of the native ligands with NHC molecules followed by removal of excess ligands by precipitation and washing, the NHC-stabilized AuNPs exhibit great long term stability in aqueous media, as shown in Fig. 1B.[29] Thus, as controlled etching reagents the above compounds may perform better.

Density functional theory (DFT) calculations

DFT calculations carried out starting with Au nanoclusters of varying number of atoms allowed us to provide further support to our experimental data. Computational details are given in ESI.† DFT calculations were used to evaluate the binding energies and bond distance (Å) of our NHC (or thiol) ligands for several nanoclusters made with fixed number of Au core atoms, where the NHC- (or thiol)-bound gold atom was allowed to relax. Structures of NHC and thiol-appended ligands are provided in ESI, Fig. S7.† Clusters of different sizes, namely, 20, 23, 26, 32, 36 and 42 Au atoms were tested for modeling the faces of the nanocolloids, in order to gain better insight into the predicted binding energy. Twelve Au atoms in the first layer were kept constant, while the second and third layers were allowed to change while monitoring energy convergence. The calculated binding energy and bond length of each NHC-modified or thiol-modified cluster of Au atoms are summarized in Table S2.†

The computed average binding energy and bond length for NHC-modified Au surfaces are 54.4 ± 2.3 kcal mol^{-1} (2.36 ± 0.1 eV) and 2.31 ± 0.01 Å, respectively. These values are within the range of binding energies and bond lengths calculated for other NHC–gold complexes.[5,48,49,90] Similarly, the calculated average binding energy and bond length for thiol-modified Au surfaces are 34.5 ± 1.39 kcal mol^{-1} (1.50 ± 0.06 eV) and 2.68 ± 0.02 Å. Note that the calculated S–Au bond energy is fully consistent with the experimental value (30 kcal mol^{-1}) from the Scoles's group.[91] Our calculated binding energy of S–Au is also in good agreement with literature data.[5,92] In addition, the average binding energy of 0.086 ± 0.004 Hartrees was achieved for NHC–Au system where the average binding energy of thiol–Au was 0.055 ± 0.002 Hartrees. Overall, our calculation though limited has allowed us to gain further insight into the differences in both bonding energy and bond length between coordination of NHC–Au and S–Au for several core size nanoclusters. They confirm the validity of the experimental data, which consistently showed higher coordination binding of NHC molecules onto Au nanocrystals compared to thiol-appended ligands. It would be interesting and informative to expand such calculation to characterize the bond energy and bond length of mutli-coordinating NHC-ligands (*e.g.*, NHC-PIMA-PEG polymers), where cooperative binding and higher affinity of such ligands to Au nanocolloids have been proven (see data shown in Fig. 1).

Conclusion

In summary, we have demonstrated that strong coordination of N-heterocyclic carbene molecules onto AuNPs can promote destabilization of the NP surfaces when large excess of ligands combined with longer incubation time are used. In particular, we found that the high affinity coordination of monoNHC-PEG can ultimately produce a near complete digestion of AuNPs. Additionally, we assessed the kinetics of the AuNP digestion by tracking changes in the UV-vis absorption profiles as a function of ligand concentration and incubation time. This allowed us to extract a relationship between the digestion rate and the molar excess of the ligand used together with the strength of the coordination interactions, *e.g.*, thiol *vs.* NHC and mono- *vs.* multi-coordinating ligands.

We applied a combination of analytical techniques, such as NMR, MALDI mass spectrometry and TEM measurements, to characterize the coordination interactions of the ligands with the AuNPs and the chemical nature of the generated NHC–Au complexes following NP digestion. We have found that the etched/digested NPs produce monoNHC- as well as bisNHC–Au complexes. We further investigated changes in the digestion kinetics when NHCs were replaced with monothiol- and dithiol-appended ligands, or when monomeric ligands were substituted with a multi-coordinating NHC-polymer. Our findings add new understanding of the coordination interactions between various Lewis base molecules and transition metal nanoparticles. They provide further understanding of why optimized incubation conditions followed by removal of excess ligands is necessary for achieving better long-term colloidal stability. Higher coordinating ligands, such as multi-coordinating polymers, alleviate this etching process and help impart better stability. This approach should be expanded to other metal core nanoparticles, which should provide better understanding of the entropic stabilization of nanocolloids in general.

Conflicts of interest

There are no conflicts of interest to declare.

Acknowledgements

We thank FSU and the National Science Foundation (NSF-CHE #2005079), AFOSR (Grant No. FA9550-18-1-0144), the National Institutes of Health (NIH #RO1DK133464), and Kasei-Asahi for financial support. We also thank Xinsong Lin and Dinesh Mishra for technical and materials support and suggestions. This research used resources provided by the Materials Characterization Laboratory at the FSU Department of Chemistry and Biochemistry (FSU075000MAC). The TEM experiments were performed at the National High Magnetic Field Laboratory, which is supported by National Science Foundation Cooperative Agreement No. DMR-1644779 and the State of Florida.

References

1 A. J. Arduengo, III, R. L. Harlow and M. Kline, A stable crystalline carbene, *J. Am. Chem. Soc.*, 1991, **113**, 361–363.
2 A. J. Arduengo, III, H. V. R. Dias, R. L. Harlow and M. Kline, Electronic stabilization of nucleophilic carbenes, *J. Am. Chem. Soc.*, 1992, **114**, 5530–5534.
3 M. N. Hopkinson, C. Richter, M. Schedler and F. Glorius, An overview of N-heterocyclic carbenes, *Nature*, 2014, **510**(7506), 485–496.
4 A. Bakker, A. Timmer, E. Kolodzeiski, M. Freitag, H. Y. Gao, H. Mönig, S. Amirjalayer, F. Glorius and H. Fuchs, Elucidating the binding modes of N-heterocyclic carbenes on a gold surface, *J. Am. Chem. Soc.*, 2018, **140**, 11889–11892.
5 S. Engel, E.-C. Fritz and B. J. Ravoo, New trends in the functionalization of metallic gold: from organosulfur ligands to N-heterocyclic carbenes, *Chem. Soc. Rev.*, 2017, **46**, 2057–2075.
6 C. A. Smith, M. R. Narouz, P. A. Lummis, I. Singh, A. Nazemi, C.-H. Li and C. M. Crudden, N-Heterocyclic, Carbenes in Materials Chemistry, *Chem. Rev.*, 2019, **119**, 4986–5056.
7 A. V. Zhukhovitskiy, M. J. MacLeod and J. A. Johnson, Carbene Ligands in Surface Chemistry: From Stabilization of Discrete Elemental Allotropes to Modification of

Nanoscale and Bulk Substrates, *Chem. Rev.*, 2015, **115**, 11503–11532.
8 P. Bellotti, M. Koy, M. N. Hopkinson and F. Glorius, Recent advances in the chemistry and applications of N-heterocyclic carbenes, *Nat. Rev. Chem.*, 2021, **5**, 711–725.
9 M. Koy, P. Bellotti, M. Das and F. Glorius, N-Heterocyclic, carbenes as tunable ligands for catalytic metal surfaces, *Nat. Catal.*, 2021, **4**, 352–363.
10 A. Gómez-Suárez, D. J. Nelson and S. P. Nolan, Quantifying and understanding the steric properties of N-heterocyclic carbenes, *Chem. Commun.*, 2017, **53**, 2650–2660.
11 H. V. Huynh, Electronic Properties of N-Heterocyclic Carbenes and Their Experimental Determination, *Chem. Rev.*, 2018, **118**, 9457–9492.
12 T. Scattolin and S. P. Nolan, Synthetic routes to late transition metal–NHC complexes, *Trends Chem.*, 2020, **2**, 721–736.
13 R. Ye, A. V. Zhukhovitskiy, R. V. Kazantsev, S. C. Fakra, B. B. Wickemeyer, F. D. Toste and G. A. Somorjai, Supported Au Nanoparticles with N-Heterocyclic Carbene Ligands as Active and Stable Heterogeneous Catalysts for Lactonization, *J. Am. Chem. Soc.*, 2018, **140**, 4144–4149.
14 H. Shen, Q. Wu, S. Malola, Y.-Z. Han, Z. Xu, R. Qin, X. Tang, Y.-B. Chen, B. K. Teo, H. Häkkinen and N. Zheng, N-Heterocyclic, Carbene-Stabilized Gold Nanoclusters with Organometallic Motifs for Promoting Catalysis, *J. Am. Chem. Soc.*, 2022, **144**, 10844–10853.
15 R. J. Lewis, M. Koy, M. Macino, M. Das, J. H. Carter, D. J. Morgan, T. E. Davies, J. B. Ernst, S. J. Freakley, F. Glorius and G. J. Hutchings, N-Heterocyclic, Carbene Modified Palladium Catalysts for the Direct Synthesis of Hydrogen Peroxide, *J. Am. Chem. Soc.*, 2022, **144**, 15431–15436.
16 J. B. Ernst, S. Muratsugu, F. Wang, M. Tada and F. Glorius, Tunable Heterogeneous Catalysis: N-Heterocyclic Carbenes as Ligands for Supported Heterogeneous Ru/K-Al_2O_3 Catalysts To Tune Reactivity and Selectivity, *J. Am. Chem. Soc.*, 2016, **138**, 10718–10721.
17 J. B. Ernst, C. Schwermann, G.-i. Yokota, M. Tada, S. Muratsugu, N. L. Doltsinis and F. Glorius, Molecular Adsorbates Switch on Heterogeneous Catalysis: Induction of Reactivity by N-Heterocyclic Carbenes, *J. Am. Chem. Soc.*, 2017, **139**, 9144–9147.
18 P. Lara, O. Rivada-Wheelaghan, S. Conejero, R. Poteau, K. Philippot and B. Chaudret, Ruthenium Nanoparticles Stabilized by N-Heterocyclic Carbenes: Ligand Location and Influence on Reactivity, *Angew. Chem., Int. Ed.*, 2011, **50**, 12080–12084.
19 C. Richter, K. Schaepe, F. Glorius and B. J. Ravoo, Tailor-made N-heterocyclic carbenes for nanoparticle stabilization, *Chem. Commun.*, 2014, **50**, 3204–3207.
20 A. Ferry, K. Schaepe, P. Tegeder, C. Richter, K. M. Chepiga, B. J. Ravoo and F. Glorius, Negatively charged N-heterocyclic carbene-stabilized Pd and Au nanoparticles and efficient catalysis in water, *ACS Catal.*, 2015, **5**, 5414–5420.
21 A. Rühling, K. Schaepe, L. Rakers, B. Vonhören, P. Tegeder, B. J. Ravoo and F. Glorius, Modular Bidentate Hybrid NHC–Thioether Ligands for the Stabilization of Palladium Nanoparticles in Various Solvents, *Angew. Chem., Int. Ed.*, 2016, **55**, 5856–5860.
22 K. V. Ranganath, J. Kloesges, A. H. Schäfer and F. Glorius, Asymmetric nanocatalysis: N–heterocyclic carbenes as chiral modifiers of Fe3O4/Pd nanoparticles, *Angew. Chem., Int. Ed.*, 2010, **49**, 7786–7789.
23 K. V. Ranganath, A. H. Schäfer and F. Glorius, Comparison of Superparamagnetic Fe3O4–Supported N–Heterocyclic Carbene–Based Catalysts for Enantioselective Allylation, *ChemCatChem*, 2011, **3**, 1889–1891.
24 J.-F. Soule, H. Miyamura and S. Kobayashi, Copolymer-incarcerated nickel nanoparticles with N-heterocyclic carbene precursors as active cross-linking agents for Corriu–Kumada–Tamao reaction, *J. Am. Chem. Soc.*, 2013, **135**, 10602–10605.
25 M. D. de Los Bernardos, S. Pérez-Rodríguez, A. Gual, C. Claver and C. Godard, Facile synthesis of NHC-stabilized Ni nanoparticles and their catalytic application in the Z-selective hydrogenation of alkynes, *Chem. Commun.*, 2017, **53**, 7894–7897.
26 M. J. MacLeod, A. J. Goodman, H.-Z. Ye, H. V.-T. Nguyen, T. Van Voorhis and J. A. Johnson, Robust gold nanorods stabilized by bidentate N-heterocyclic-carbene–thiolate ligands, *Nat. Chem.*, 2019, **11**, 57–63.
27 L. Du, N. A. Nosratabad, Z. Jin, C. Zhang, S. Wang, B. Chen and H. Mattoussi, Luminescent Quantum Dots Stabilized by N-Heterocyclic Carbene Polymer Ligands, *J. Am. Chem. Soc.*, 2021, **143**, 1873–1884.
28 D. E. Westmoreland, R. López-Arteaga and E. A. Weiss, N-Heterocyclic, Carbenes as Reversible Exciton-Delocalizing Ligands for Photoluminescent Quantum Dots, *J. Am. Chem. Soc.*, 2020, **142**, 2690–2696.
29 N. A. Nosratabad, Z. Jin, L. Du, M. Thakur and H. Mattoussi, N-Heterocyclic, Carbene-Stabilized Gold Nanoparticles: Mono- Versus Multidentate Ligands, *Chem. Mater.*, 2021, **33**, 921–933.
30 N. A. Nosratabad, Z. Jin, L. Du and H. Mattoussi, Colloidal Nanoparticles for Biomedical Applications XVII, in *N-Heterocyclic carbene-stabilized gold nanoparticles and luminescent quantum dots*, SPIE, 2022, pp. 8–17.
31 N. Möller, A. Rühling, S. Lamping, T. Hellwig, C. Fallnich, B. J. Ravoo and F. Glorius, Stabilization of High Oxidation State Upconversion Nanoparticles by N-Heterocyclic Carbenes, *Angew. Chem., Int. Ed.*, 2017, **56**, 4356–4360.
32 P. K. Jain, X. H. Huang, I. H. El-Sayed and M. A. El-Sayed, Noble Metals on the Nanoscale: Optical and Photothermal Properties and Some Applications in Imaging, Sensing, Biology, and Medicine, *Acc. Chem. Res.*, 2008, **41**, 1578–1586.
33 S. Barbosa, A. Agrawal, L. Rodríguez-Lorenzo, I. Pastoriza-Santos, R. A. Alvarez-Puebla, A. Kornowski, H. Weller and L. M. Liz-Marzán, Tuning Size and Sensing Properties in Colloidal Gold Nanostars, *Langmuir*, 2010, **26**, 14943–14950.

34 A. M. Alkilany, L. B. Thompson, S. P. Boulos, P. N. Sisco and C. J. Murphy, Gold nanorods: Their potential for photothermal therapeutics and drug delivery, tempered by the complexity of their biological interactions, *Adv. Drug Delivery Rev.*, 2012, **64**, 190–199.
35 L. Z. Vigderman and E. R. Zubarev, Therapeutic platforms based on gold nanoparticles and their covalent conjugates with drug molecules, *Adv. Drug Delivery Rev.*, 2013, **65**, 663–676.
36 C. Burda, X. B. Chen, R. Narayanan and M. A. El-Sayed, Chemistry and properties of nanocrystals of different shapes, *Chem. Rev.*, 2005, **105**, 1025–1102.
37 L. D. Pachón and G. Rothenberg, Transition-metal nanoparticles: synthesis, stability and the leaching issue, *Appl. Organomet. Chem.*, 2008, **22**, 288–299.
38 W. Zhou, X. Gao, D. Liu and X. Chen, Gold Nanoparticles for In Vitro Diagnostics, *Chem. Rev.*, 2015, **115**, 10575–10636.
39 K. Saha, S. S. Agasti, C. Kim, X. Li and V. M. Rotello, Gold nanoparticles in chemical and biological sensing, *Chem. Rev.*, 2012, **112**, 2739–2779.
40 F. Aldeek, M. Safi, N. Q. Zhan, G. Palui and H. Mattoussi, Understanding the Self-Assembly of Proteins onto Gold Nanoparticles and Quantum Dots Driven by Metal-Histidine Coordination, *ACS Nano*, 2013, **7**, 10197–10210.
41 A. Kapur, F. Aldeek, X. Ji, M. Safi, W. Wang, A. Del Cid, O. Steinbock and H. Mattoussi, Self-Assembled Gold Nanoparticle–Fluorescent Protein Conjugates as Platforms for Sensing Thiolate Compounds via Modulation of Energy Transfer Quenching, *Bioconjugate Chem.*, 2017, **28**, 678–687.
42 Z. Jin, N. Dridi, G. Palui, V. Palomo, J. V. Jokerst, P. E. Dawson, Q.-X. Amy Sang and H. Mattoussi, Evaluating the Catalytic Efficiency of the Human Membrane-type 1 Matrix Metalloproteinase (MMP-14) Using AuNP–Peptide Conjugates, *J. Am. Chem. Soc.*, 2023, **145**, 4570–4582.
43 M. K. Corbierre, N. S. Cameron and R. B. Lennox, Polymer-stabilized gold nanoparticles with high grafting densities, *Langmuir*, 2004, **20**, 2867–2873.
44 M.-T. Lee, C.-C. Hsueh, M. S. Freund and G. S. Ferguson, Air oxidation of self-assembled monolayers on polycrystalline gold: the role of the gold substrate, *Langmuir*, 1998, **14**, 6419–6423.
45 N. Bhatt, P.-J. J. Huang, N. Dave and J. Liu, Dissociation and degradation of thiol-modified DNA on gold nanoparticles in aqueous and organic solvents, *Langmuir*, 2011, **27**, 6132–6137.
46 C. M. Crudden, J. H. Horton, M. R. Narouz, Z. Li, C. A. Smith, K. Munro, C. J. Baddeley, C. R. Larrea, B. Drevniok and B. Thanabalasingam, Simple direct formation of self-assembled N-heterocyclic carbene monolayers on gold and their application in biosensing, *Nat. Commun.*, 2016, **7**, 1–7.
47 P. A. Redhead, Thermal desorption of gases, *Vacuum*, 1962, **12**, 203–211.
48 A. V. Zhukhovitskiy, M. G. Mavros, T. Van Voorhis and J. A. Johnson, Addressable Carbene Anchors for Gold Surfaces, *J. Am. Chem. Soc.*, 2013, **135**, 7418–7421.
49 P. Pyykkö and N. Runeberg, Comparative Theoretical Study of N-Heterocyclic Carbenes and Other Ligands Bound to AuI, *Chem. – Asian J.*, 2006, **1**, 623–628.
50 A. Antušek, M. Blaško, M. Urban, P. Noga, D. Kisić, M. Nenadović, D. Lončarević and Z. Rakočević, Density functional theory modeling of C–Au chemical bond formation in gold implanted polyethylene, *Phys. Chem. Chem. Phys.*, 2017, **19**, 28897–28906.
51 M. Rodríguez-Castillo, G. Lugo-Preciado, D. Laurencin, F. Tielens, A. van der Lee, S. Clément, Y. Guari, J. M. López-de-Luzuriaga, M. Monge, F. Remacle and S. Richeter, Experimental and Theoretical Study of the Reactivity of Gold Nanoparticles Towards Benzimidazole-2-ylidene Ligands, *Chem. – Eur. J.*, 2016, **22**, 10446–10458.
52 M. Rodríguez-Castillo, D. Laurencin, F. Tielens, A. van der Lee, S. Clément, Y. Guari and S. Richeter, Reactivity of gold nanoparticles towards N-heterocyclic carbenes, *Dalton Trans.*, 2014, **43**, 5978–5982.
53 E. C. Hurst, K. Wilson, I. J. Fairlamb and V. Chechik, N-Heterocyclic, carbene coated metal nanoparticles, *New J. Chem.*, 2009, **33**, 1837–1840.
54 G. Wang, A. Rühling, S. Amirjalayer, M. Knor, J. B. Ernst, C. Richter, H.-J. Gao, A. Timmer, H.-Y. Gao, N. L. Doltsinis, F. Glorius and H. Fuchs, Ballbot-type motion of N-heterocyclic carbenes on gold surfaces, *Nat. Chem.*, 2017, **9**, 152–156.
55 Z. Jin, L. Du, C. Zhang, Y. Sugiyama, W. Wang, G. Palui, S. Wang and H. Mattoussi, Modification of Poly(maleic anhydride)-Based Polymers with H2N–R Nucleophiles: Addition or Substitution Reaction?, *Bioconjugate Chem.*, 2019, **30**, 871–880.
56 B. C. Mei, E. Oh, K. Susumu, D. Farrell, T. J. Mountziaris and H. Mattoussi, Effects of Ligand Coordination Number and Surface Curvature on the Stability of Gold Nanoparticles in Aqueous Solutions, *Langmuir*, 2009, **25**, 10604–10611.
57 W. Wang, X. Ji, L. Du and H. Mattoussi, Enhanced Colloidal Stability of Various Gold Nanostructures Using a Multicoordinating Polymer Coating, *J. Phys. Chem. C*, 2017, **121**, 22901–22913.
58 M. H. Stewart, K. Susumu, B. C. Mei, I. L. Medintz, J. B. Delehanty, J. B. Blanco-Canosa, P. E. Dawson and H. Mattoussi, Multidentate Poly(ethylene glycol) Ligands Provide Colloidal Stability to Semiconductor and Metallic Nanocrystals in Extreme Conditions, *J. Am. Chem. Soc.*, 2010, **132**, 9804–9813.
59 Z. Jin, Y. Sugiyama, C. Zhang, G. Palui, Y. Xin, L. Du, S. Wang, N. Dridi and H. Mattoussi, Rapid Photoligation of Gold Nanocolloids with Lipoic Acid-Based Ligands, *Chem. Mater.*, 2020, **32**, 7469–7483.
60 H. Hiramatsu and F. E. Osterloh, A simple large-scale synthesis of nearly monodisperse gold and silver nanoparticles with adjustable sizes and with exchangeable surfactants, *Chem. Mater.*, 2004, **16**, 2509–2511.
61 S. Liu, G. Chen, P. N. Prasad and M. T. Swihart, Synthesis of monodisperse Au, Ag, and Au–Ag alloy nanoparticles

with tunable size and surface plasmon resonance frequency, *Chem. Mater.*, 2011, **23**, 4098–4101.
62 D. Mishra, S. Wang, Z. Jin, Y. Xin, E. Lochner and H. Mattoussi, Highly fluorescent hybrid Au/Ag nanoclusters stabilized with poly(ethylene glycol)- and zwitterion-modified thiolate ligands, *Phys. Chem. Chem. Phys.*, 2019, **21**, 21317–21328.
63 D. Tapu, D. A. Dixon and C. Roe, ^{13}C NMR spectroscopy of "Arduengo-type" carbenes and their derivatives, *Chem. Rev.*, 2009, **109**, 3385–3407.
64 A. J. Arduengo III, D. A. Dixon, K. K. Kumashiro, C. Lee, W. P. Power and K. W. Zilm, Chemical shielding tensor of a carbene, *J. Am. Chem. Soc.*, 1994, **116**, 6361–6367.
65 A. R. Chianese, B. M. Zeglis and R. H. Crabtree, Unexpected oxidative C–C cleavage in the metallation of 2-substituted imidazolium salts to give N-heterocyclic carbene complexes, *Chem. Commun.*, 2004, 2176–2177.
66 D. Marchione, M. A. Izquierdo, G. Bistoni, R. Havenith, A. Macchioni, D. Zuccaccia, F. Tarantelli and L. Belpassi, ^{13}C NMR spectroscopy of N-heterocyclic carbenes can selectively probe σ donation in gold(I) complexes, *Chem. – Eur. J.*, 2017, **23**, 2722–2728.
67 C. S. Cazin, *N-Heterocyclic carbenes in transition metal catalysis and organocatalysis*, Springer Science & Business Media, 2010, vol. 32.
68 S. Thanneeru, K. M. Ayers, M. Anuganti, L. Zhang, C. V. Kumar, G. Ung and J. He, N-Heterocyclic, carbene-ended polymers as surface ligands of plasmonic metal nanoparticles, *J. Mater. Chem. C*, 2020, **8**, 2280–2288.
69 L. Zhang, Z. Wei, M. Meng, G. Ung and J. He, Do polymer ligands block the catalysis of metal nanoparticles? Unexpected importance of binding motifs in improving catalytic activity, *J. Mater. Chem. A*, 2020, **8**, 15900–15908.
70 V. Lewe, M. Preuss, E. Woźnica, D. Spitzer, R. Otter and P. Besenius, A clickable NHC–Au (I)-complex for the preparation of stimulus-responsive metallopeptide amphiphiles, *Chem. Commun.*, 2018, **54**, 9498–9501.
71 M. E. Garner, W. Niu, X. Chen, I. Ghiviriga, K. A. Abboud, W. Tan and A. S. Veige, N-heterocyclic carbene gold(I) and silver(I) complexes bearing functional groups for bio-conjugation, *Dalton Trans.*, 2015, **44**, 1914–1923.
72 P. DeFrémont, R. Singh, E. D. Stevens, J. L. Petersen and S. P. Nolan, Synthesis, characterization and reactivity of N-heterocyclic carbene gold(III) complexes, *Organometallics*, 2007, **26**, 1376–1385.
73 N. Goswami, K. Zheng and J. Xie, Bio-NCs–the marriage of ultrasmall metal nanoclusters with biomolecules, *Nanoscale*, 2014, **6**, 13328–13347.
74 A. Munir, K. S. Joya, T. Ul Haq, N. U. A. Babar, S. Z. Hussain, A. Qurashi, N. Ullah and I. Hussain, Metal nanoclusters: new paradigm in catalysis for water splitting, solar and chemical energy conversion, *ChemSusChem*, 2019, **12**, 1517–1548.
75 M. A. Habeeb Muhammed, S. Ramesh, S. S. Sinha, S. K. Pal and T. Pradeep, Two distinct fluorescent quantum clusters of gold starting from metallic nanoparticles by pH-dependent ligand etching, *Nano Res.*, 2008, **1**, 333–340.
76 E. A. Martynova, N. V. Tzouras, G. Pisano, C. S. Cazin and S. P. Nolan, The "weak base route" leading to transition metal–N-heterocyclic carbene complexes, *Chem. Commun.*, 2021, **57**, 3836–3856.
77 J. M. Azcue, *Environmental impacts of mining activities: emphasis on mitigation and remedial measures*, Springer Science & Business Media, 2012.
78 C. S. Weisbecker, M. V. Merritt and G. M. Whitesides, Molecular self-assembly of aliphatic thiols on gold colloids, *Langmuir*, 1996, **12**, 3763–3772.
79 L. Du, W. Wang, C. Zhang, Z. Jin, G. Palui and H. Mattoussi, A versatile coordinating ligand for coating semiconductor, metal, and metal oxide nanocrystals, *Chem. Mater.*, 2018, **30**, 7269–7279.
80 G. Palui, T. Avellini, N. Zhan, F. Pan, D. Gray, I. Alabugin and H. Mattoussi, Photoinduced Phase Transfer of Luminescent Quantum Dots to Polar and Aqueous Media, *J. Am. Chem. Soc.*, 2012, **134**, 16370–16378.
81 P. Pallavicini, L. Preti, L. D. Vita, G. Dacarro, Y. A. Diaz Fernandez, D. Merli, S. Rossi, A. Taglietti and B. Vigani, Fast dissolution of silver nanoparticles at physiological pH, *J. Colloid Interface Sci.*, 2020, **563**, 177–188.
82 H. W. Duan and S. M. Nie, Etching colloidal gold nanocrystals with hyperbranched and multivalent polymers: A new route to fluorescent and water-soluble atomic clusters, *J. Am. Chem. Soc.*, 2007, **129**, 2412–2213.
83 M. A. Habeeb Muhammed, P. K. Verma, S. K. Pal, A. Retnakumari, M. Koyakutty, S. Nair and T. Pradeep, Luminescent Quantum Clusters of Gold in Bulk by Albumin-Induced Core Etching of Nanoparticles: Metal Ion Sensing, Metal-Enhanced Luminescence, and Biolabeling, *Chem. – Eur. J.*, 2010, **16**, 10103–10112.
84 F. Bosse, C. Gutheil, D. T. Nguyen, M. Freitag, M. Das, B. J. Tyler, T. Adolphs, A. H. Schäfer, H. F. Arlinghaus, F. Glorius and B. J. Ravoo, Selective Removal of Gold: N-Heterocyclic Carbenes as Positive Etch Resists on Planar Gold Surfaces, *ACS Appl. Mater. Interfaces*, 2023, **15**, 36831–36838.
85 S. R. Isaacs, E. C. Cutler, J.-S. Park, T. R. Lee and Y.-S. Shon, Synthesis of tetraoctylammonium-protected gold nanoparticles with improved stability, *Langmuir*, 2005, **21**, 5689–5692.
86 L. Cau, P. Deplano, L. Marchiò, M. L. Mercuri, L. Pilia, A. Serpe and E. F. Trogu, New powerful reagents based on dihalogen/N,N′-dimethylperhydrodiazepine-2,3-dithione adducts for gold dissolution: the IBr case, *Dalton Trans.*, 2003, (10), 1969–1974.
87 S. Singh and B. L. V. Prasad, Nearly Complete Oxidation of Au° in Hydrophobized Nanoparticles to Au3+ Ions by N-Bromosuccinimide, *J. Phys. Chem. C*, 2007, **111**, 14348–14352.
88 P. Yang and X. Zhang, Nucleic acid-mediated gold oxidation: novel biolithography for surface microfabrication and new insight into gold-based biomaterials, *Chem. Commun.*, 2012, **48**, 8787–8789.

89 X. Liu, Y. Wang, L. Xiao, L. Ma, P. Han and S. Ye, Eco-friendly and rapid extraction of gold by *in situ* catalytic oxidation with N-bromosuccinimide, *Heliyon*, 2022, **8**, e09706.
90 X. Xu, S. H. Kim, X. Zhang, A. K. Das, H. Hirao and S. H. Hong, Abnormal N-heterocyclic carbene gold(I) complexes: synthesis, structure, and catalysis in hydration of alkynes, *Organometallics*, 2013, **32**, 164–171.
91 D. J. Lavrich, S. M. Wetterer, S. L. Bernasek and G. Scoles, Physisorption and chemisorption of alkanethiols and alkyl sulfides on Au (111), *J. Phys. Chem. B*, 1998, **102**, 3456–3465.
92 P. D. Jadzinsky, G. Calero, C. J. Ackerson, D. A. Bushnell and R. D. Kornberg, Structure of a Thiol Monolayer-Protected Gold Nanoparticle at 1.1 Å Resolution, *Science*, 2007, **318**, 430–433.